International Journal of Engineering Research and Science & Technology

IJERST

ISSN : 2319-5991

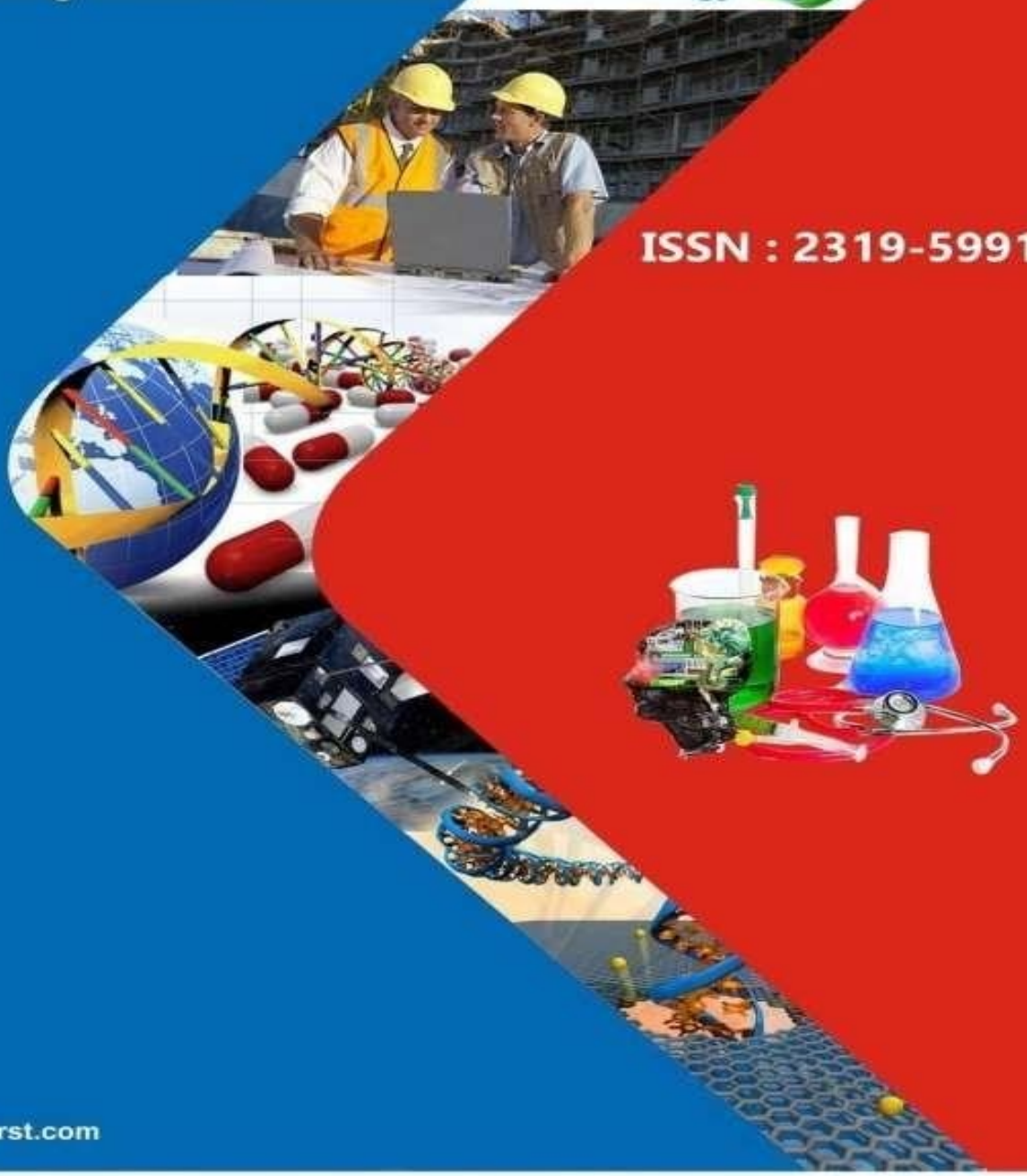

www.ijerst.com

Email: editor@ijerst.com or editor.ijerst@gmail.com

International Journal of Engineering Research and Science & Technology

ISSN 2319-5991 www.ijerst.com

Vol. 20, Issue 1, 2024

Mechanical characteristics of auxetic composite honeycomb sandwich structureunder bending

Mr. A. Venkateshan, Mr. C. Jegadeeswaran, Dr. S. Gayathri, Mr. A. Ramkumar

Associate Professor [3], Assistant Professor [1,2,4]

venkateshan.k@actechnology.in, cjegadeseswaran@actechnology.in, gayathiri.s@actechnology.in, ramkumar.a@actechnology.in

Department of Civil, Arjun College of Technology, Thamaraikulam, Coimbatore-Pollachi Highway, Coimbatore, Tamilnadu-642 120

Abstract

In comparison to conventional non-auxetic sandwich structures (TNS), AHS made of a single material often show reduced platform stress and energy absorption (EA). To overcome this drawback, this research looks at the re-entrant honeycomb sandwich structure's (RS) usage of aluminium foam (AF) as a filler. While the auxetic composite honeycomb sandwich structure successfully resolves interface delamination seen in conventional non-auxetic composite sandwich structures, filling the AHS with AF considerably increases the EA and platform stress compared to filling the TNS with AF. After that, designs that reinforce the mechanical properties of a single honeycomb sandwich structure are presented using positive-negative Poisson's ratio coupling. By capitalising on the hexagonal honeycomb's high bearing capacity and the considerable contact between the re-entrant honeycomb and the filler material, the coupling structure optimises the mechanical characteristics, according to the analytical findings. Protective engineering stands to benefit greatly from the suggested auxetic composite honeycomb sandwich structures, since they outperform conventional non-auxetic sandwich constructions in terms of EA and platform stress.

Keywords: Auxetic, Energy absorption, Mechanical metamaterial, Aluminum foam, Re-entrant, Three-point bending

1 Introduction

The sandwich structure is widely used in protective engineering due to its outstanding specific stiffness and energy absorption (EA) properties. It consists of a lightweight core material sandwiched between rigid stiff face-sheets (Bohara et al., 2023; Ma et al., 2021; Wang et al., 2022; Xia et al., 2022a, 2022b; Zhang et al., 2023). Core and sandwich mechanical characteristics are affected by core and sandwich geometrical parameters. front sheets. (Boonkong et al., 2016; Rubino et al., 2010; Vidwans et al., 2023; Yan et al., 2022), among many others, cores may be Y-shaped, made of metal foam, or arranged in a honeycomb pattern. Honeycomb sandwich constructions stand out from the others because of its exceptional EA, increased stiffness, and increased strength. For their 2019 study, He et al. combined low-speed impact testing with three-point flexural testing to look at how residual bending strength and impact-induced damage traits affectedSandwich panels made of honeycomb. This was determined by Wang et al. The ceramic sandwich becomes indented in the region immediately around the two supports that are bent (Wang et al., 2019a, 2019b). Subsequent research by Wang et al. (2019a, 2019b) found that the geometric arrangement significantly affected the bending performance of ceramic honeycomb sandwich panels. The engineered

International Journal of Engineering Research and Science & Technology

ISSN 2319-5991 www.ijerst.com

Vol. 20, Issue 1, 2024

Sun et al. (2021) examined the characteristics of short-aramid-fiber sandwich panels under varying loading velocities. In addition, Neresh et al. (2021) compared the flexure and mechanical characteristics of sandwich structures using standard sandwich panels that have a single core with those that incorporate numerous honeycomb cores. The researched sandwich designs mostly include either a single homogeneous material or many composite layers, which is worth noting. But this doesn't change the fact that the core material can only support so much weight. Mechanically, honeycomb sandwich constructions packed with pliable materials are preferable to multi-layer composites. This is because, in a composite honeycomb sandwich plate, the filler is embedded in the honeycomb core, which causes the two materials to generate extra contact forces. A comparative investigation of several types of corrugated sandwich panels revealed that adding polyurethane foam greatly improves the EA (Hamidin et al., 2021). The non-auxetic honeycomb structure may cause interface delamination due to its small interaction impact with the interior filler material. Mechanical meta-materials with a negative Poisson's ratio, or "auxet-ics" (Evans et al., 1991), have the peculiar property of swelling under compression and shrinking under stretching (Asad et al., 2020; Coulais et al., 2018; Pan et al., 2024). Their unique behaviour distinguishes them from traditional engineering materials and generates a robust interaction between auxetics and the interior filling components (Lv et al., 2020; Zhao et al., 2021). Auxetics' better EA qualities have prompted a lot of research and early uses in protective engineering areas, including honeycomb sandwich constructions (Xia et al., 2022a, 2022b), and other similar structures (Ni et al., 2023; Foster et al., 2018; Ren et al., 2018). An extensive examination of the bending reaction and failure causes was carried out in a work on designed graded cellular structures (Hou et al., 2013). Based on the architecture of the sandwich panels, the mechanical properties were shown to be significantly affected by the gradient extent and aspect ratio of the auxetic unit cells with angle gradient cores. The failure mechanism, deformation behaviour, and mechanical properties of sandwich panels with non-auxetic and auxetic honeycomb cells were examined by Li et. al. (2022) who also examined the influence of various parameters. Research by Geramizadeh et al. (2022) examined the effects of different face-sheet thicknesses on the switching failure mechanisms and EA development rate in sandwich beams. These beams included re-entrant honeycomb and hexagonal honeycomb. Later on, the effect resilience of polyurea-coated auxetic honeycomb sandwich panels was examined. The highest effective impact resistance was discovered in sandwich panels with coatings applied to the reverse side (He et al., 2023). A research project was proposed that would focus on multilayer composites with an auxetic core that was specifically constructed. The impact of thin facings on mechanical characteristics would be thoroughly examined (Peliński & Smardzewski, 2022). Keep in mind that these studies mostly deal with transverse and out-of-plane bending, and that auxetic sandwich structures have only just begun to be explored for their possibilities in longitudinal bending. Low stiffness and bearing capacity are two main obstacles to the development of auxetic structures at the moment. The broad use of auxetic structures in many domains has been hindered by these restrictions. Researchers have been looking for ways to increase overall stiffness without sacrificing the auxetic effect in order to overcome these obstacles. To improve the stability of deformation and the EA feature, Luo et al. (2022) suggested a method that combines the auxetic structure with delayed recovery foam. Afterwards, the mechanical characteristics of auxetic honey-comb filled with aluminium foam (AF) and subjected to axial compression were investigated. According to the results, the contact between the AF and auxetic honeycomb is greater than that between the non-auxetic honeycomb. Xu et al. (2023) found that the auxetic composite structure improved the EA without sacrificing its auxetic features. Although there are other types of auxetic cells, the re-entrant honeycomb has attracted a lot of attention due to its strong auxetic impact and relatively simple production procedure (Gao et al., 2020, 2023; Chen & Wang, 2022). This work aimed to enhance the mechanical properties of re-entrant honeycombs when subjected to longitudinal bending by manufacturing and studying an aluminium foam-filled re-entrant honeycomb sandwich structure (FRS). This structure, in its structural shape, corresponds to a double-layer sandwich plate (Li et al., 2023). Comparing FRS to an aluminium foam-filled hexagonal honeycomb sandwich construction (FHS) allowed researchers to examine its deformation pattern, EA property, and longitudinal bending resistance. The parameter analysis also covered how different dimensions affected the EA and bending performance. To optimise the structural mechanical properties, various connection structures were finally created and investigated.

.

2 Approach to design and fabrication

2.1 Design of basic cell

Two types of common honeycomb structures were selected for this study, namely the non-auxetic hexagonal

International Journal of Engineering Research and Science & Technology

ISSN 2319-5991 www.ijerst.com

Vol. 20, Issue 1, 2024

honeycomb and auxetic re-entrant honeycomb according to the configuration of basic cells (Fig. 1). In order to facilitate a fair comparison between the two cell types, an identical rectangular design layout was employed for both. The size parameters of basic cells are displayed in Table 1 to provide a clear understanding of their characteristics.

In this work, a two-step process was utilized to integrate the face-sheets and core of the sandwich structure as depicted in Fig. 2. Initially, the two types of

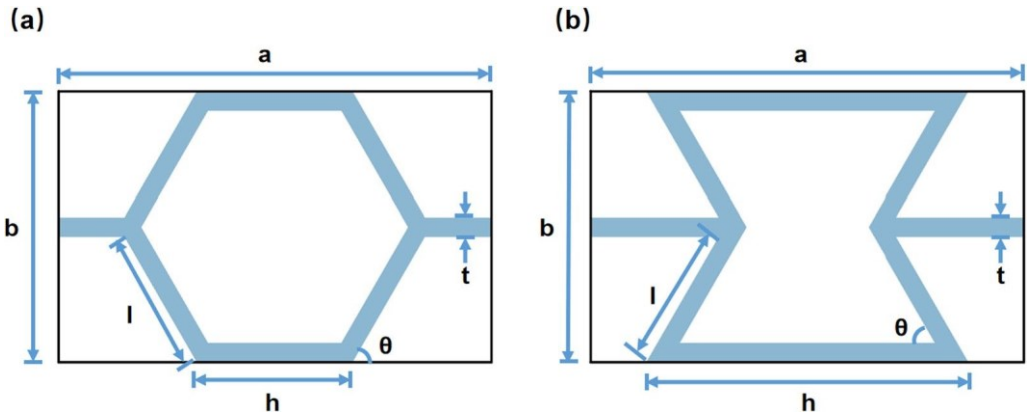

Fig. 1 Geometrical dimensions of the basic cell of **a** hexagonal honeycomb and **b** re-entrant honeycomb

Table 1 Geometrical parameters of the basic cells

Specimen	*a* (mm)	*b* (mm)	*h* (mm)	*l* (mm)	*t* (mm)	*θ* (°)	Porosity (%)	Relative density (%)
Re-entrant	22.27	13.86	16.58	7.42	1.00	60	0.83	0.17
Hexagonal	22.27	13.86	8.00	7.42	1.00	60	0.76	0.24

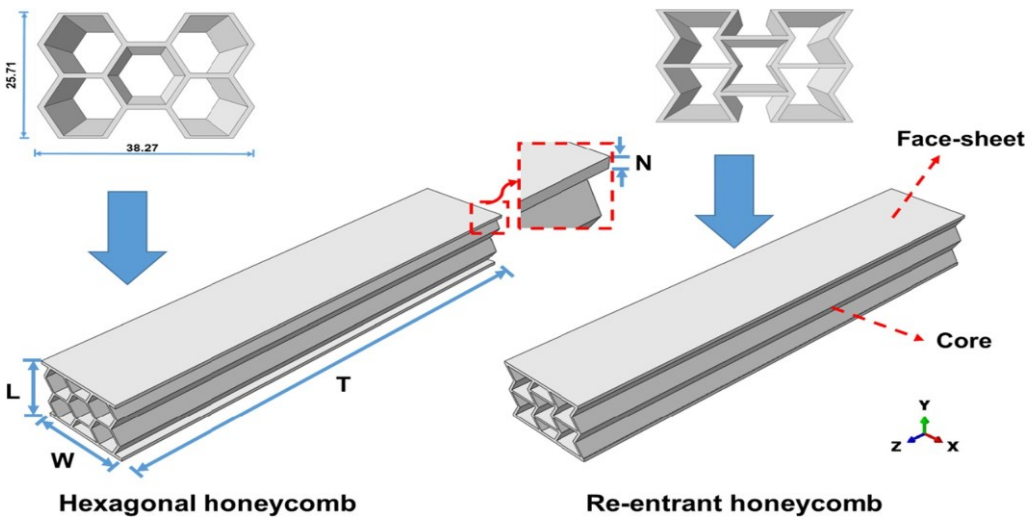

Fig. 2 The dimension of the honeycomb sections and sandwich structures

International Journal of Engineering Research and Science & Technology

ISSN 2319-5991 www.ijerst.com

Vol. 20, Issue 1, 2024

basic cells were arrayed to form honeycomb structures with 2 × 2 basic cells, all possessing identical cross-section dimensions. Subsequently, these honeycomb structures were employed as the core, with rectangular components acting as the face-sheets. This integration approach maintains the integrity and stability of the structure.

The face-sheet thickness N is 1.50 mm, and the structures with 2×2 basic cells were extended to a length of 200 mm in the Z direction. The length, width, and height of each structure are T = 200 mm, W = 38.27 mm, and L = 27.71 mm, respectively. The structures were fabricated using solid 316L stainless steel pieces by wire cutting technology. Notably, the face-sheets and core were manufactured as one unit, eliminating the need for welding or adhesive bonding.

2.2 Fabrication of aluminum foam-filled honeycombs

Aluminum foam (AF) is characterized by its highly porous structure, which imparts several advantageous properties such as low density, superior EA performance, and high specific stiffness. These remarkable properties make AF an attractive material for applications requiring energy absorption. However, the rough surface of AF poses challenges for its direct use in civil engineering and protection fields. By incorporating AF as a filler in the voids of sandwich structures, it proves to be a strategic solution in overcoming these inherent limitations, and significantly elevates the overall performance of the structures, particularly in terms of EA, damping, and acoustic performance. Therefore, in this study, AF was selected as the filling material and shaped into two types of honeycombs through wire cutting. Subsequently, the honeycomb-shaped AF was manually inserted into the respective honeycomb frames without the use of any binders (Fig. 3).

3 Characteristics of the material

3.1 Tests of stainless steel specimens

Three specimens, each 1 mm thick, were manufactured in accordance with the ASTM E8M-2004 standard for conducting a tensile test on 316L stainless steel. The dimensional details of the specimens can be observed in Fig. 4. The specimens were produced using a wire-cutting technique that utilizes electrical spark discharge between the fine wire electrode and the workpiece to melt and cut the metal with precision. The tensile testing was executed on all specimens at a constant velocity of 2 mm/min. The primary objective of performing uniaxial tensile tests on the stainless steel specimens was to derive a constitutive model. This model would subsequently be employed in simulations and parametric analyses to predict the mechanical behavior. The density of the stainless steel specimen was measured at 7930 kg/m^3. Stainless steel can be characterized by an elastic modulus of 190 GPa, a Poisson's ratio of 0.29, and a yield stress of 470.36 MPa (Fig. 5).

3.2 Tests of aluminum foam

Following the ASTM D1621-10 Standard, three cubic samples with dimensions of 50 mm × 50 mm × 50 mm (Fig. 6) were fabricated. In order to achieve the material properties of AF, samples were underwent quasi-static uniaxial compression testing using an MTS testing machine. The samples were subjected to a constant loading rate of 3 mm/min (Fig. 6). The AF material exhibited a density of 660 kg/m^3, an elastic modulus of 509.6 MPa (Fig. 7), and a plastic Poisson's ratio of 0.

4 Experimental setup and corresponding simulations

4.1 Experimental setup

The mechanical properties of four different types of sandwich structures were assessed by conducting three-point bending tests (Fig. 8), employing a universal testing machine (SUNS WDW-100). The test machine has

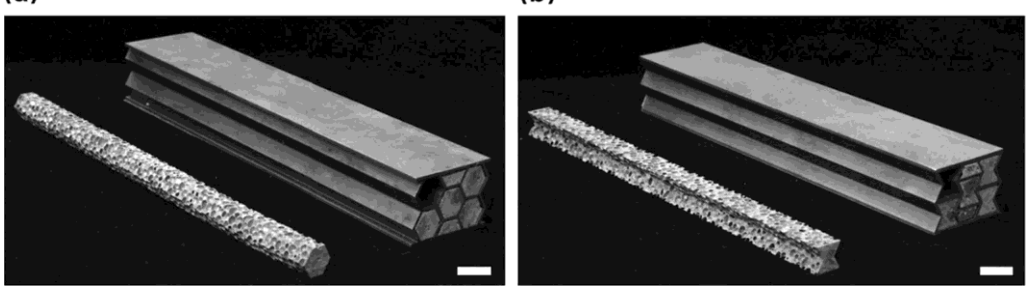

Fig. 3 **a** Manufacture of aluminum foam-filled hexagonal honeycomb sandwich structure (FHS) and **b** aluminum foam-filled re-entrant honeycomb sandwich structure (FRS) (scale bar: 20 mm)

International Journal of Engineering Research and Science & Technology

ISSN 2319-5991 www.ijerst.com

Vol. 20, Issue 1, 2024

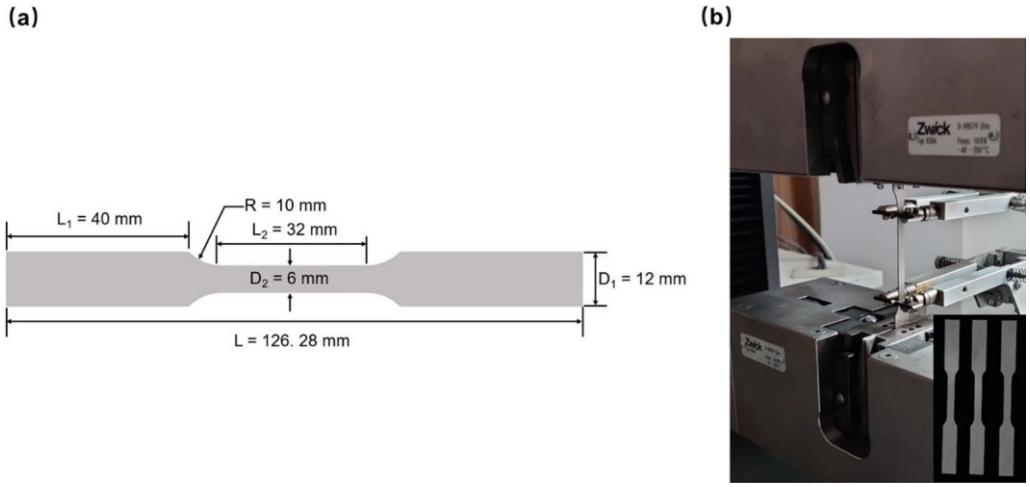

Fig. 4 **a** The specimen dimensions and **b** tensile strength testing of stainless steel samples

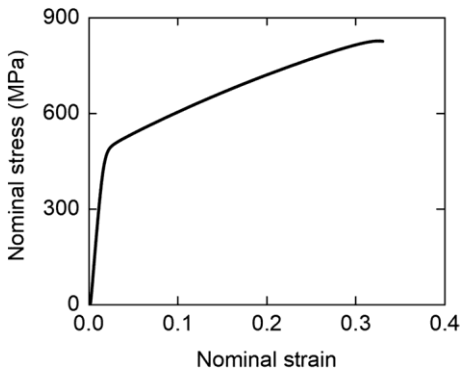

Fig. 5 Stress-strain relationship of 316L stainless steel

a maximum load capacity of 100 kN and was operated at a consistent loading speed of 3 mm/min throughout the testing process. This loading speed was chosen to mimic quasi-static loading conditions, thereby ensuring accurate measurement and analysis. Both the supports and indenter were of a 30 mm diameter ∅. The distance h of 150 mm between the two supports was maintained during the experiment. To capture the deformation behavior of the specimens during the mechanical testing, a camcorder was utilized to document the testing procedure. A schematic representation of the size parameters is provided in Fig. 8b.

Energy absorption (EA) of specimens is quantified as the total external energy that is dissipated during an impact event. This quantity is typically derived by integrating the load–deflection curve:

$$EA = \int_0^d f(x)dx, \tag{1}$$

where d is the deflection of the indenter, and $f(x)$ is the correlation between load and deflection.

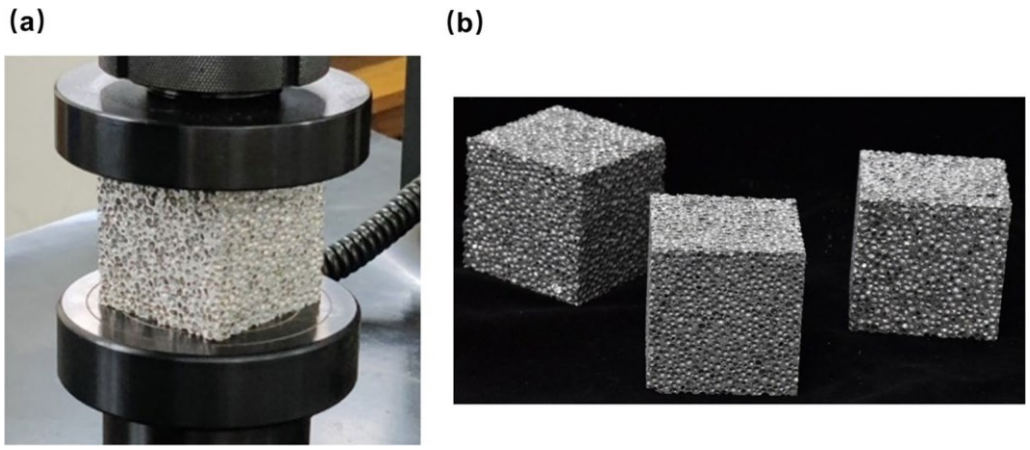

Fig. 6 **a** Compressive strength testing of aluminum foam (AF) and **b** three cubic samples of AF

International Journal of Engineering Research and Science & Technology

ISSN 2319-5991 www.ijerst.com

Vol. 20, Issue 1, 2024

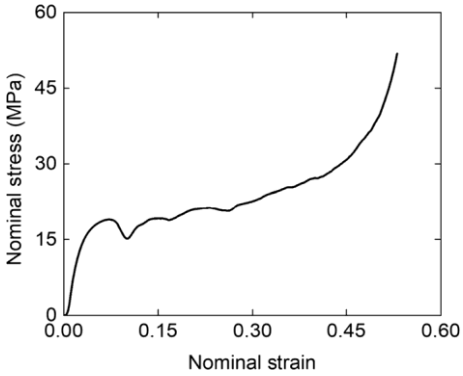

Fig. 7 Stress-strain relationship of AF

Specific energy absorption (SEA) is defined as the EA per unit mass. It is typically calculated by dividing the EA by the weight of the structural component.

$$SEA = \frac{EA}{m}. \quad (2)$$

Peak crushing force (PCF) refers to the maximum force during bending. As a protective structure, it is unfavorable when the value of PCF is too large. Mean crushing force (MCF) indicates the EA per unit displacement b of the indenter.

$$MCF = \frac{EA}{b}. \quad (3)$$

Crush force efficiency (CFE) is the ratio of the MCF to the PCF and is always used to measure the protection ability of a structure. The greater the CFE value, the higher the protective effect.

$$CFE = \frac{MCF}{PCF}. \quad (4)$$

4.2 Finite element simulations

To further assess the mechanical property of the structures, finite element models were generated with identical dimensions to those used in the experiments and numerical simulations. These models were analyzed using Abaqus/Explicit 6.14, a commercial finite element software solver. To capture the behavior of the stainless steel, an isotropic elastic–plastic model was employed, and the material parameters were obtained from the tensile test from Sect. 3.1. For the analysis of the AF, a crushable foam material model was utilized, and the material parameter was deduced from the compression test described in Sect. 3.2. To simulate the compression process, the structure was subjected to compression between two analytical rigid bodies: supports and an indenter. To facilitate the application of boundary conditions, three reference points were placed in both the supports and the indenter, which facilitates adding the arrangement of boundary conditions. The supports were fixed and the indenter underwent a displacement of 18 mm. General contact properties were employed for interactions between various components in the simulation. This encompasses contacts between the indenter and structures, supports and structures, as well as the structures and AF. A tangential friction coefficient of 0.3 was specifically assigned to accurately simulate the interactions between the components. Moreover, normal contact was modeled as hard contact to mitigate penetration of the structural elements.

A hexahedral mesh (C3D8R) is utilized for numerical modeling of both the honeycomb sandwich structures and the AF. To achieve an optimal mesh distribution, a symmetric gradient mesh approach was adopted after performing a convergence analysis of the RS and AF. This approach involved increasing the mesh density in regions characterized by high stress concentration (such as near

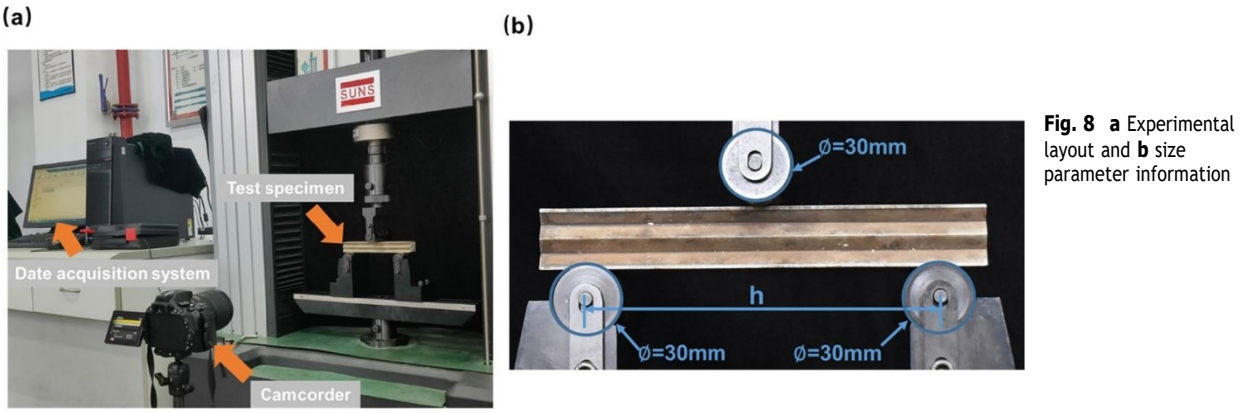

Fig. 8 **a** Experimental layout and **b** size parameter information

International Journal of Engineering Research and Science & Technology

ISSN 2319-5991 www.ijerst.com

Vol. 20, Issue 1, 2024

the indenter) and decreasing the mesh density in other parts (Fig. 9). The approximate global mesh size for the honeycomb sandwich structures was set as 0.35 mm. Additionally, the element size of the AF mesh was determined to be 1.5 mm. These specific configurations can balance computational efficiency and accuracy.

5 Results and discussion

Upon subjecting the specimens to an indenter displacement of 18 mm, the deformation patterns of four different sandwich structures were obtained, as illustrated in Fig. 10. Despite the manifestation of cracks in proximity to the center of the bottom face-sheet of the re-entrant honeycomb sandwich structure (RS) during the experiment, the observed overall experimental deformation pattern corresponded well with the numerical simulations. This manifestation can be attributed to defects in the wire-cutting process. Notably, in the process of bending, the AF was noticeably squeezed out of the honeycomb to a greater extent in FRS in comparison to the hexagonal honeycomb sandwich structure (HS). This behavior is likely due to the more effective interaction between the AF and the RS in contrast to the HS.

To demonstrate the deformation patterns of the mid-span sections, finite element analysis was employed, yielding deformation patterns as depicted by the red dashed lines in Fig. 10. Due to the auxetic effect, the auxetic core of the RS shrinks inward, while the non-auxetic core in the HS squeezes and bends to both sides. Similarly, the auxetic core exhibits an inward contraction mechanism, thereby imposing constraints on the adjacent AF inside the FRS due to the auxetic effect. However, conspicuous interface delamination is observed in the FHS, indicating incomplete interfacial contact between the non-auxetic core and the AF.

The parameter denoted as the bending angle θ (Fig. 11) represents the angular deviation between the bottom face-sheet and the horizontal plane of the structure. A larger bending angle denotes a more pronounced curvature at the two ends of the structure.

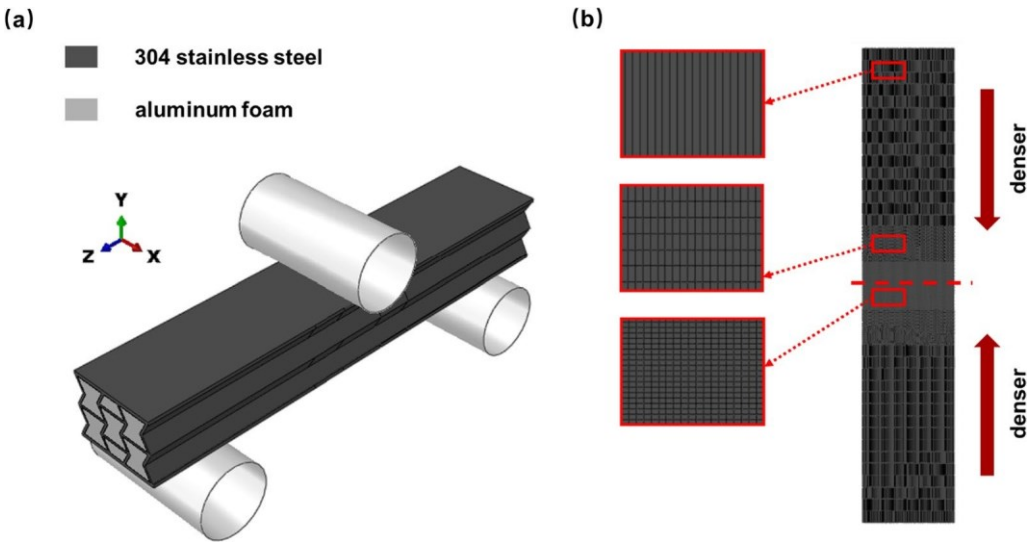

Fig. 9 **a** Finite element model and **b** gradient mesh (detail in red lines) of the RS

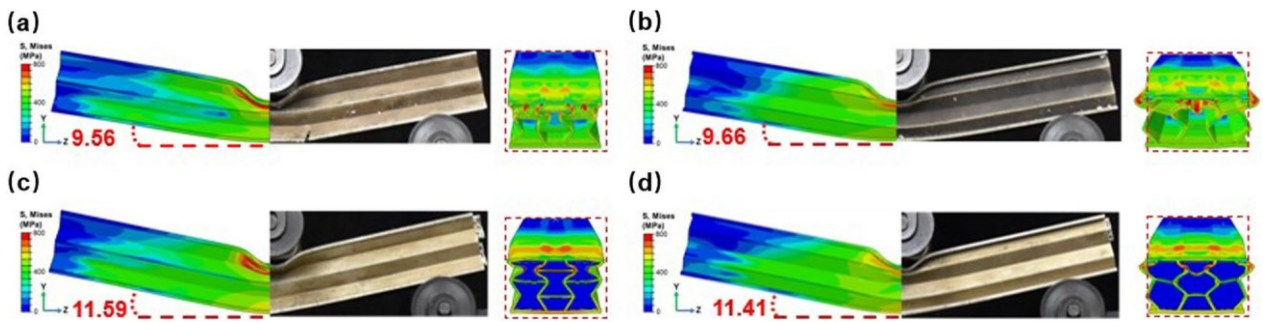

Fig. 10 Deformation patterns and mid-span sections (in red dashed lines) for **a** RS, **b** HS, **c** FRS, and **d** FHS

International Journal of Engineering Research and Science & Technology

ISSN 2319-5991 www.ijerst.com

Vol. 20, Issue 1, 2024

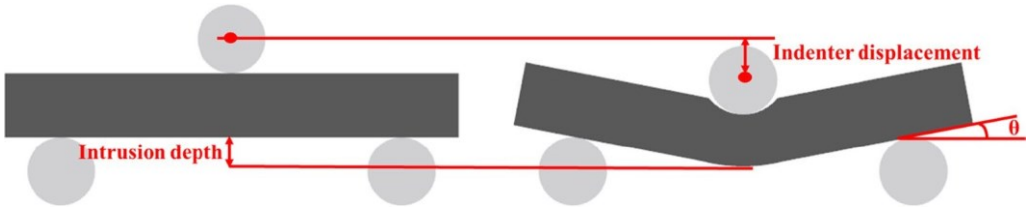

Fig. 11 Illustration of the bending angle θ and the intrusion depth

For the RS and HS specimens, the bending angles are measured at 9.56° and 9.66°, respectively, which indicates that HS produces a more pronounced bending. Following the infusion with AF, the bending angles for the FRS and FHS configurations are determined as 11.59° and 11.41°, respectively, representing an increase in bending angles post-treatment. The intrusion depth is another index to reflect the flexural performance of the structures, wherein a greater intrusion depth stands for heightened bending, primarily localized at the midpoint of the structures (Xia et al., 2022a, 2022b). In this study, the term "intrusion depth" (Fig. 11) refers to the displacement observed at the midpoint of the bottom face-sheet when the indenter displacement attains 18 mm. The simulation results reveal intrusion depths of 9.45 mm, 9.39 mm, 12.49 mm and 11.85 mm for RS, HS, FRS, and FHS, respectively. It can be observed that the intrusion depth undergoes a substantial increase after filling the AF.

The comparison of the load–deflection curves for four distinct structures subjected to three-point bending and computational simulation is depicted in Fig. 12. In this study, deflection specifically denotes the indenter deflection. The bending response observed in the experimental data aligns well with the finite element curve across the four different honeycomb sandwich structures, including elastic modulus and platform stress, indicating a consistent correlation between experimental data and finite element analysis results. However, owing to the transverse bending (Fig. 15) of the bottom face-sheet, the simulation curve exhibits a slightly greater magnitude than the experimental curve at the later stage of deformation subsequent to being filled with AF.

An obvious difference in the boundary conditions (Fig. 13) between the experiment and the simulation is noted in the vicinity of the indenter. In the simulation setting, the indenter is completely immersed in the upper face-sheet, whereas in the experimental setup, the

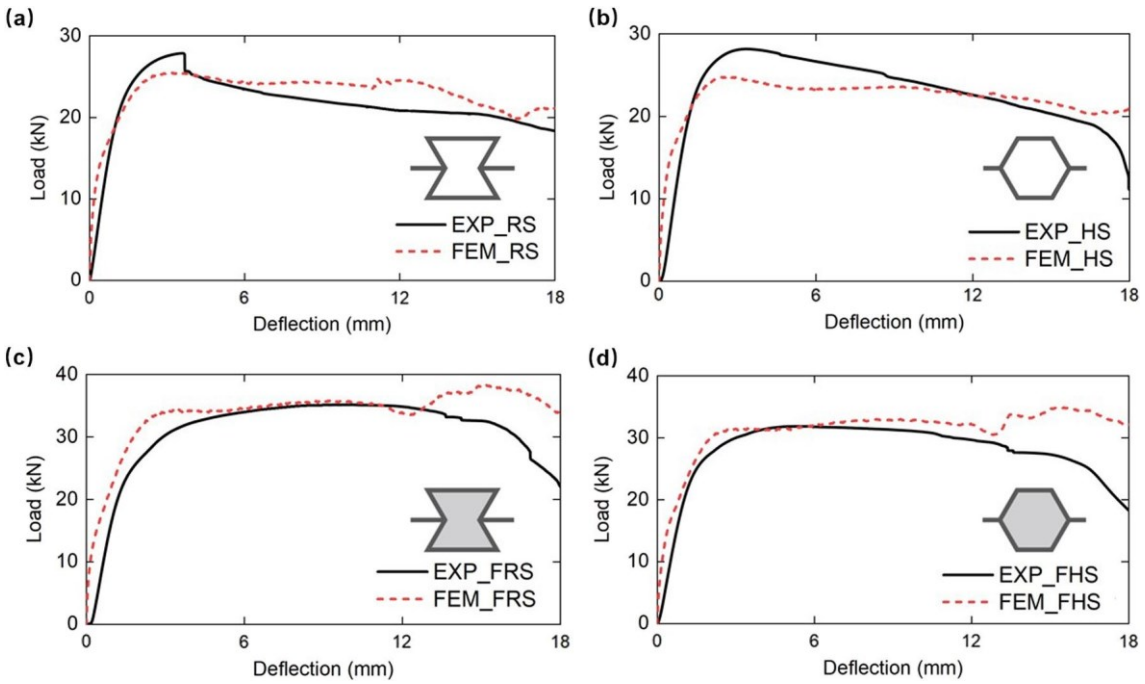

Fig. 12 Comparison of the load-deflection curves for **a** RS, **b** HS, **c** FRS and **d** FHS between simulations and experiments

International Journal of Engineering Research and Science & Technology

ISSN 2319-5991 www.ijerst.com

Vol. 20, Issue 1, 2024

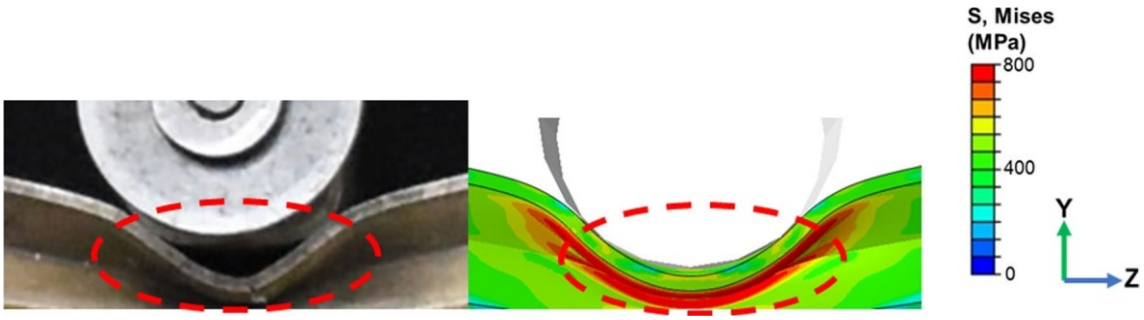

Fig. 13 Difference in boundary conditions between the experiment and the simulation

indenter does not establish complete contact with the upper face-sheet. This variance may be ascribed to the inherent imperfections present in the experimental materials relative to the ideal conditions assumed in the simulation. As a result, the bending angles derived from the experimental data are slightly larger than those predicted by the simulation.

The platform stage of the structures achieves stabilization post-filling, but the bearing capacity of FRS manifests a more substantial increment compared to that of FHS. This observed phenomenon underscores the superior performance of the interaction between the auxetic honeycomb and the AF. This can be interpreted as the auxetic honeycomb restraining the deformation of AF, while the AF provides support for the auxetic honeycomb.

Unlike quasi-static compression, the SEA of RS is lower than that of HS (Table 2), because only part of the structure is deformed during bending. However, the SEA of RS surpasses that of HS upon the incorporation of AF into both kinds of honeycomb sandwich structures. Although SEA of FRS is slightly larger than that of FHS, their respective improvements post AF filling exhibit distinguishable characteristics.

The enhanced factor of EA of the structure post AF filling is defined as α through the formula:

$$\alpha = \frac{EA_2 - EA_1}{EA_1}, \tag{5}$$

where EA_1 and EA_2 are the values of energy absorption for the hollow and composite sandwich structures, respectively.

Likewise, the enhanced factor is extended to SEA, characterized as β according to the formula:

$$\beta = \frac{SEA_2 - SEA_1}{SEA_1}, \tag{6}$$

Table 2 Correlation between simulated and experimental mechanical properties in RS, HS, FRS and FHS

Design	Intrusion depth (mm)	Bending angle (°)	EA (J)	SEA (J/g)
EXP-RS	–	10.24	387.997	0.866
FEM-RS	9.45	9.56	413.425	0.92
EXP-HS	–	10.03	409.110	1.010
FEM-HS	9.39	9.66	401.648	0.99
EXP-FRS	–	11.81	552.150	1.026
FEM-FRS	12.49	11.59	608.881	1.132
EXP-FHS	–	12.01	500.960	1.004
FEM-FHS	11.85	11.41	562.720	1.128

where SEA_1 and SEA_2 are the values of specific energy absorption for the hollow and composite sandwich structures, respectively.

α (EA) and β (SEA) of FRS stand at 0.47 and 0.23 respectively, while those of FHS are measured at 0.40 and 0.14. Both enhanced factors of FRS are larger than those of FHS. Moreover, FRS exhibits a propensity for a larger cell count which subsequently results in an increased bending area, particularly enhancing its applicability in engineering scenarios. These findings underscore the superior performance of the re-entrant composite structure in bending situations compared with conventional composite honeycomb structures.

6 Finite element analyses

6.1 Finite element model validation

The numerical load–deflection curves obtained from the simulation bear a high level of consistency with the experimental outcomes as presented in Sect. 5. Compared with FHS, FRS has advantages in terms of EA and deformation pattern. Therefore, a parametric analysis of FRS is conducted in this section. The subsequent sections delve into the impact of the face-sheet thickness and the cell wall thickness. To qualitatively analyze the EA capacity of structures, five distinct energy absorption indices

International Journal of Engineering Research and Science & Technology

ISSN 2319-5991 www.ijerst.com

Vol. 20, Issue 1, 2024

are proposed, i.e., EA, mean crushing force (MCF), peak crushing force (PCF), crush force efficiency (CFE), and SEA. The bending performance is predominantly assessed based on the intrusion depth and bending angle.

6.2 Parametric studies of cell wall thickness

The sandwich structures' primary function is to absorb energy during the bending process, with the core playing a critical role as the main energy absorber. Consequently, the mechanical features of these structures are significantly affected by the geometrical parameters of the basic cell of the honeycomb core. In order to investigate the influence of the geometrical parameters of cells on the mechanical properties, four different cell wall thicknesses (1.0 mm, 1.4 mm, 1.8 mm, and 2.2 mm) were individually set, while keeping other parameters constant.

Figure 14 presents the patterns of structural deformation and mid-span sections for various cell wall thicknesses. As the cell wall thickness increases, both intrusion depth and bending angle (Table 3) of the structures significantly increase, indicating a more pronounced bending of the structure. The mid-span sections further reveal that a thicker cell wall diminishes the structural compressibility, thereby indicating a weakening of the auxetic effect.

The load–deflection curves of the four kinds of structures are displayed as Fig. 15. As the thickness of the cell wall is augmented, there is a commensurate enhancement in the stiffness of the structure. An evident peak force manifests initially when the thickness of the cell wall reaches 1.8 mm. Nevertheless, it is imperative to note that a substantial rise in the initial peak force is deemed unfavorable in the field of engineering protection.

An increase in cell wall thicknesses causes the progression of transverse bending in the bottom facesheet. From the load–deflection curves, it is observable that the displacement during the second strengthening stage (deflection after the star) advances.

Elevated cell wall thicknesses result in higher EA and SEA values for the structures (Table 3). However, the increment in SEA gradually diminishes. This phenomenon may be elucidated by postulating that heightened cell wall thicknesses would lead to reduced filler content, as well as a decrease in the available shrinkage space of the AF. In addition, a notable surge in the value of PCF accompanies increments in cell wall thickness, thereby compromising the delicate balance between injury tolerance and EA capacity in protective engineering.

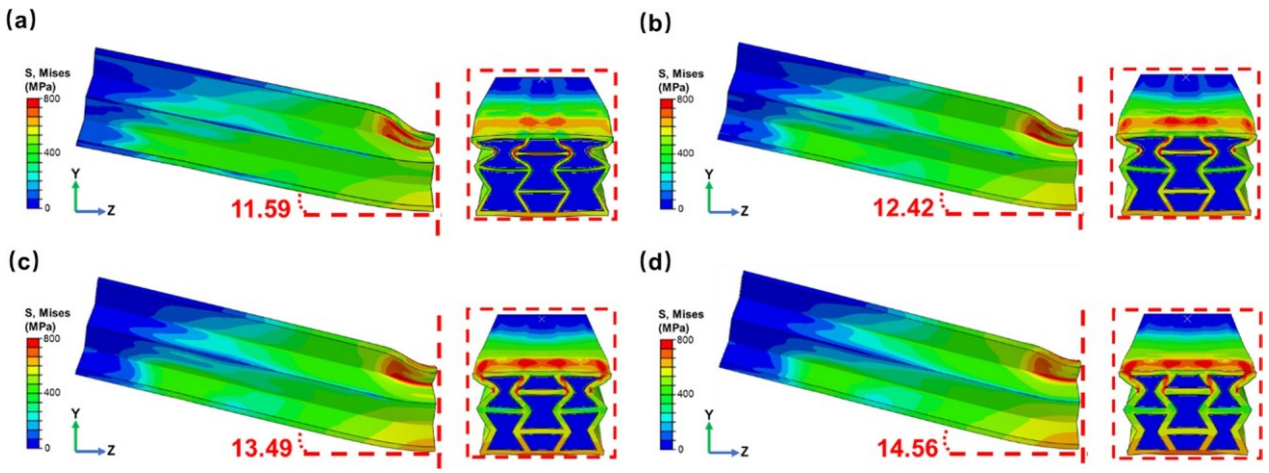

Fig. 14 Deformation patterns and mid-span sections in simulation for **a** 1.0 mm, **b** 1.4 mm, **c** 1.8 mm and **d** 2.2 mm

Table 3 Mechanical features of FRSs with varying cell wall thicknesses

Design	Intrusion depth (mm)	Bending angle (°)	EA (J)	MCF (kN)	PCF (kN)	CFE (%)	SEA (J/g)
1.0 mm	12.49	11.59	608.88	33.83	38.34	0.88	1.132
1.4 mm	13.57	12.42	766.05	42.56	49.99	0.85	1.214
1.8 mm	14.60	13.49	919.67	51.09	60.42	0.85	1.276
2.2 mm	15.40	14.56	1064.59	59.14	69.85	0.85	1.316

International Journal of Engineering Research and Science & Technology

ISSN 2319-5991 www.ijerst.com

Vol. 20, Issue 1, 2024

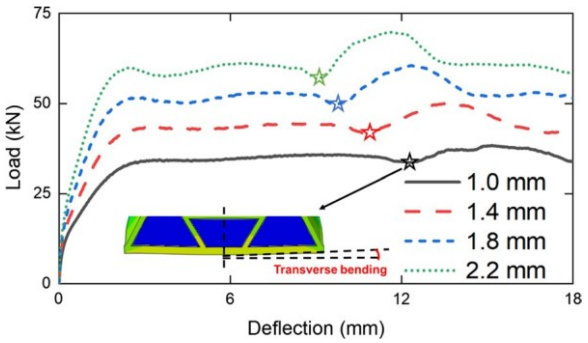

Fig. 15 Load-deflection curves of FRSs with various cell wall thicknesses (the stars in the figure indicate the beginning of transverse bending in the bottom face-sheet)

6.3 Parametric studies of face-sheet thickness

Considering that the face-sheet of the sandwich structure is the most severely bent part, this component serves as a critical determinant of the overall mechanical properties of the structure. To explore the correlation between face-sheet thickness and mechanical features, distinct face-sheet thicknesses of 1.2 mm, 1.5 mm, 1.8 mm, and 2.1 mm were examined, while maintaining consistent dimensions for other structural components.

The deformation patterns and mid-span sections with various face-sheet thicknesses are illustrated in Fig. 16. Both intrusion depth and bending angle (Table 4) of the structures exhibit a pronounced decrease as face-sheet thickness increases. This phenomenon signifies an enhancement in the structure's resistance to bending. Notably, analysis of the mid-span sections reveals that changes in face-sheet thickness yield minimal impact on the auxetic effect (Fig. 16).

From the load–deflection curves of the four sandwich structures displayed in Fig. 17, it is evident that the stiffness E and the platform stress of the structure exhibit an uptrend as the thickness of the face sheets increases, albeit the increase is relatively small. Observations of the load–deflection curves indicate a postponed onset of the secondary strengthening phase, implying that an increase in face-sheet thickness leads to a retardation in transverse bending in the bottom face-sheet.

After analysis, it is found that the trend of SEA exhibits an initial rise followed by a subsequent decline. This phenomenon underscores that a judicious augmentation in face-sheet thickness yields an amplification in SEA.

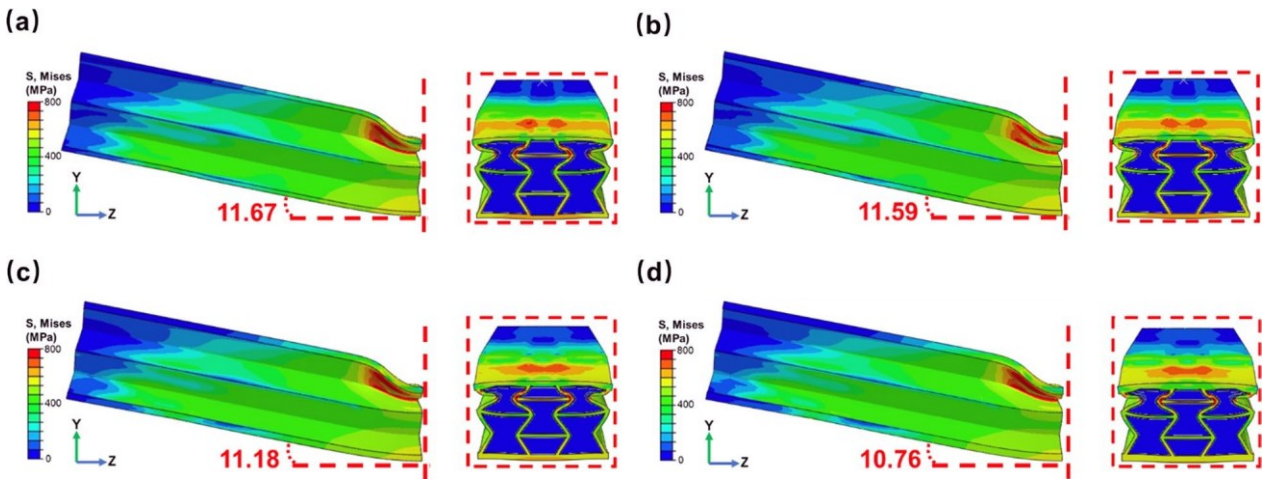

Fig. 16 Deformation patterns and mid-span sections in simulation for **a** 1.2 mm, **b** 1.5 mm, **c** 1.8 mm and **d** 2.1 mm

Table 4 Mechanical features of FRSs with varying face-sheet thicknesses

Design	Intrusion depth (mm)	Bending angle (°)	EA (J)	MCF (kN)	PCF (kN)	CFE (%)	SEA (J/g)
1.2 mm	12.56	11.67	598.95	33.28	38.37	0.87	1.126
1.5 mm	12.49	11.59	608.88	33.83	38.34	0.88	1.132
1.8 mm	12.16	11.18	638.06	35.45	38.85	0.91	1.123
2.1 mm	11.99	10.76	669.87	37.22	39.97	0.93	1.120

International Journal of Engineering Research and Science & Technology

ISSN 2319-5991 www.ijerst.com

Vol. 20, Issue 1, 2024

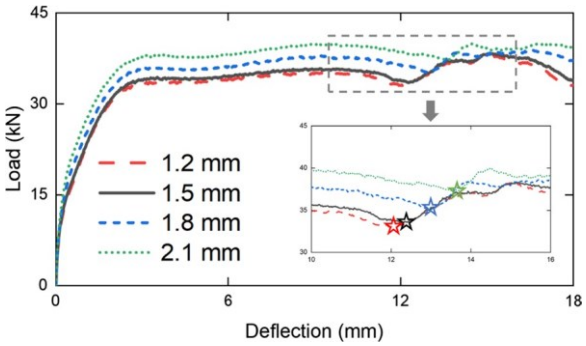

Fig. 17 Load-deflection curves of FRSs with various face-sheet thicknesses

However, the essential role of the face-sheet is to resist bending rather than absorb energy. Correspondingly, the increase of face-sheet thickness will inevitably reduce both the proportion of the internal honeycomb structure and the amount of filler material. Thus, it is evident that an excessive increase in the thickness of face-sheet will compromise the SEA performance of the overall structure.

6.4 Positive–negative Poisson's ratio coupling structures

As analyzed in Sect. 5, the SEA of HS is higher than that of RS. However, following the introduction of fillings, the SEA of FRS exceeds that of FHS. This discrepancy can be attributed to the phenomenon of interface delamination occurring between the AF and the non-auxetic honeycomb inside the FHS. Such delamination indicates that the interaction force between the AF and the non-auxetic honeycomb is much smaller in comparison to those observed in the auxetic honeycomb. In order to mitigate the issue of interface delamination in FHS and enhance the EA performance, this section attempts to combine the auxetic honeycomb with the non-auxetic honeycomb to design a positive–negative Poisson's ratio coupling structure. Specifically, novel coupling architectures featuring a confluence of 1 × 2 non-auxetic honeycomb and 1 × 2 auxetic honeycomb are designed and investigated, as illustrated in Fig. 18. The cell dimensions of both honeycomb types adhere to the previously specified parameters, encompassing the three-dimensional dimensions of the structure, and the relative positions of the two kinds of honeycomb are also compared and analyzed.

Both the intrusion depth and bending angle of the newly designed positive–negative Poisson's ratio coupling structures exhibit modest increments compared to those of the FRS (Fig. 19). However, the mid-span sections of the two coupling structures align closely with the delineation represented by the red dashed lines, indicating a tangible decrease in interfacial delamination. It is worth noting that segments of AF protrude from both coupling structures owing to the reinforcement effect, with this occurrence being more pronounced in the context of FPNS.

The stiffness and platform force of FPNS are significantly enhanced when compared with those of the FRS, while the load–deflection curves of the FRS and the FNPS exhibit similarities (Fig. 20). The findings confirm that the relative positions of non-auxetic honeycomb and auxetic honeycomb affect the mechanical features of the coupling structure. The bearing capacity of the non-auxetic frame is greater than that of the auxetic frame, thus enabling FPNS to withstand higher pres- sure levels during bending. Subsequent to the filling of foam, interface delamination manifests in the non- auxetic honeycomb, leading to a decrease in platform force. This occurrence can be mitigated through the reasonable combination of the two honeycomb types, thereby elucidating the benefits of FPNS. Moreover, both EA and SEA of FPNS are enhanced through the employment of this coupling methodology (Table 5).

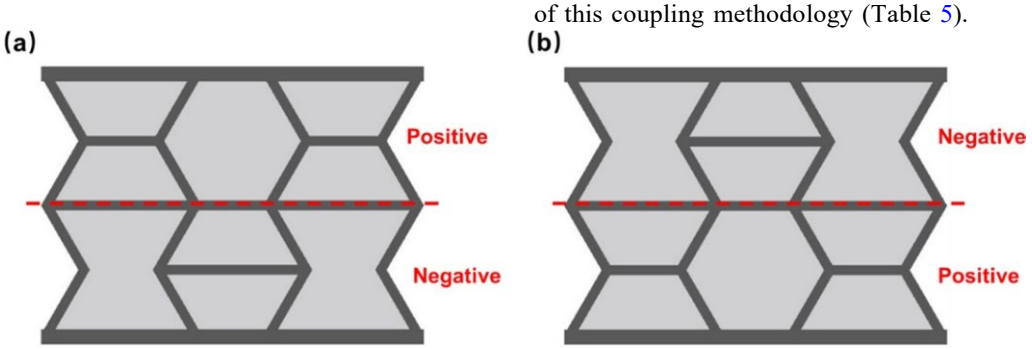

Fig. 18 The comparison of structural diagram for **a** aluminum foam-filled positive-negative Poisson's ratio coupling sandwich structure (FPNS) and **b** aluminum foam-filled negative-positive Poisson's ratio coupling sandwich structure (FNPS)

International Journal of Engineering Research and Science & Technology

ISSN 2319-5991 www.ijerst.com

Vol. 20, Issue 1, 2024

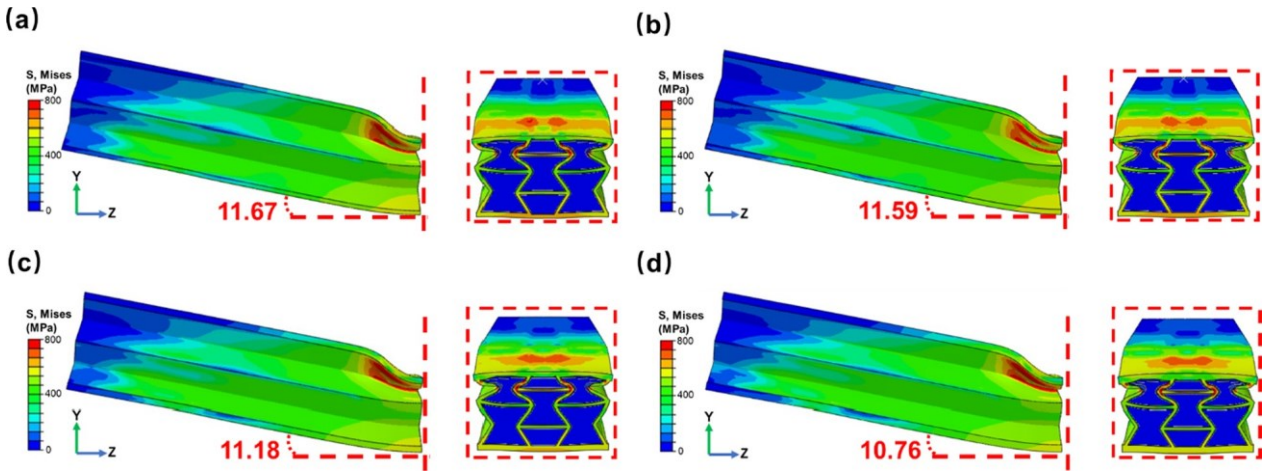

Fig. 19 Deformation patterns and mid-span sections in simulation for **a** FRS, **b** FHS, **c** FPNS and **d** FNPS

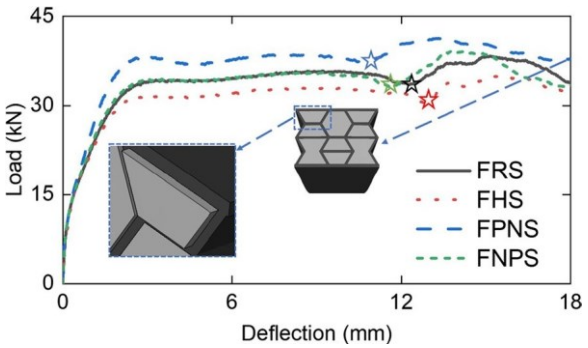

Fig. 20 Comparison of load-deflection curves of FRS, FHS, FPNS (AF is extruded out in blue dashed lines) and FNPS

7 Conclusions

In this study, we introduce a novel composite architecture comprising a re-entrant honeycomb sandwich structure (RS) integrated with aluminum foam (AF). Through a combination of simulations and experimental analyses, we investigate the bending properties, deformation pattern and energy absorption (EA) properties of this composite structure. The findings indicate that the aluminum foam-filled re-entrant honeycomb sandwich structure (FRS) exhibits notable advantages in terms of superior EA performance and enhanced deformation behavior.

Furthermore, we conduct a comprehensive parametric analysis to elucidate the interplay between cell wall thickness, face-sheet thickness, and FRS. By assessing two key metrics, namely bending resistance and specific energy absorption (SEA), guidelines for optimal design are established. Within a specific range, increasing cell wall thickness leads to a reduction in bending resistance but a corresponding enhancement in SEA. Conversely, raising face-sheet thickness improves bending resistance but reduces SEA. Leveraging insights from the parametric study, we propose an optimized design configuration featuring a face-sheet thickness of 1.5 mm and a cell wall thickness of 1.0 mm. Lastly, our integrated design approach underscores the benefits of auxetic materials, which not only mitigate interface delamination but also enhance EA performance under a three-point bending load.

The proposed structure exhibits superior EA and deformation characteristics compared to monolithic materials and non-auxetic composite sandwich configurations. These desirable findings herald the potential of auxetic materials in advancing protective engineering applications.

Table 5 Mechanical features of FRS, FHS, FPNS and FNPS

Design	Intrusion depth (mm)	Bending angle (°)	EA (J)	MCF (kN)	PCF (kN)	CFE (%)	SEA (J/g)
FRS	12.49	11.59	608.88	33.83	38.34	88	1.132
FHS	11.85	11.41	562.72	31.26	34.96	89	1.128
FPNS	13.64	11.84	666.07	37.00	41.40	89	1.218
FNPS	12.95	11.72	608.20	33.79	39.16	86	1.112

International Journal of Engineering Research and Science & Technology

ISSN 2319-5991 www.ijerst.com

Vol. 20, Issue 1, 2024

Acknowledgements
This work was supported by the National Natural Science Foundation of China (Grant Number 51978330); Qing Lan Project of Jiangsu Province; Natural Science Foundation of Jiangsu Province (Grant Number BK20220103).

Author contributions
All authors participated in the study and supported the publication. Hang Hang Xu: conceptualization, methodology, software, writing original draft. Xue Gang Zhang: investigation, validation, editing. Dong Han: investigation, validation, editing. Wei Jiang: investigation, validation. Yi Zhang: investigation, validation, editing. Yu Ming Luo: investigation, validation, editing. Xi Hai Ni: investigation, validation, editing. Xing Chi Teng: investigation, validation, editing. Yi Min Xie: validation, editing. Xin Ren: conceptualization, methodology, project administration, supervision, funding acquisition, editing, revision. All authors read and approved the final manuscript.

Data availability
All data generated or analyzed during this study are included in this article. Further inquiries can be directed to the corresponding author.

Declarations

Consent for publication
The manuscript is approved by all authors for publication.

Competing interests
The authors declare no competing interests.

Received: 12 December 2023 Revised: 30 March 2024 Accepted: 4 April 2024
Published online: 14 May 2024

References

Asad, M., Dhanasekar, M., Zahra, T., & Thambiratnam, D. (2020). Impact mitigation of masonry walls with carbon fibre and auxetic fibre composite renders—A numerical study. *Structures, 28*, 2733-2751. https://doi.org/10.1016/j.istruc.2020.09.047

Bohara, R. P., Linforth, S., Nguyen, T., Ghazlan, A., & Ngo, T. (2023). Anti-blast and -impact performances of auxetic structures: A review of structures, materials, methods, and fabrications. *Engineering Structures, 276*, 115377.

Boonkong, T., Shen, Y. O., Guan, Z. W., & Cantwell, W. J. (2016). The low velocity impact response of curvilinear-core sandwich structures. *International Journal of Impact Engineering, 93*, 28-38. https://doi.org/10.1016/j.ijimpeng.2016.01.012

Chen, Y., & Wang, Z. W. (2022). In-plane elasticity of the re-entrant auxetic hexagonal honeycomb with hollow-circle joint. *Aerospace Science and Technology, 123*, 107432. https://doi.org/10.1016/j.ast.2022.107432

Coulais, C., Sabbadini, A., Vink, F., & van Hecke, M. (2018). Multi-step self-guided pathways for shape-changing metamaterials. *Nature, 561*, 512-515. https://doi.org/10.1038/s41586-018-0541-0

Evans, K. E., Nkansah, M. A., Hutchinson, I. J., & Rogers, S. C. (1991). Molecular network design. *Nature, 353*, 124. https://doi.org/10.1038/353124a0

Foster, L., Peketi, P., Allen, T., Senior, T., Duncan, O., & Alderson, A. (2018). Application of auxetic foam in sports helmets. *Applied Sciences, 8*, 354. https://doi.org/10.3390/app8030354

Gao, Q., Li, W. B., Shi, Y., Liao, W.-H., Yin, G. D., Li, J. W., Wang, C. Y., & Qiu, R. X. (2023). A rotating auxetic energy harvester for vehicle wheels. *Engineering Structures, 288*, 116190. https://doi.org/10.1016/j.engstruct.2023.116190

Gao, Q., Liao, W.-H., & Wang, L. (2020). An analytical model of cylindrical double-arrowed honeycomb with negative Poisson's ratio. *International Journal of Mechanical Sciences, 173*, 105400. https://doi.org/10.1016/j.ijmecsci.2019.105400

Geramizadeh, H., Dariushi, S., & Salami, S. J. (2022). Optimal face sheet thickness of 3D printed polymeric hexagonal and re-entrant honeycomb sandwich beams subjected to three-point bending. *Composite Structures, 291*, 115618. https://doi.org/10.1016/j.compstruct.2022.115618

Hamidin, F., Farrokhabadi, A., & Ahmadi, H. (2021). The effect of core shape on the bending response of sandwich panels with filled and unfilled sine and square corrugated cores. *Journal of Failure Analysis and Prevention, 21*, 537-546. https://doi.org/10.1007/s11668-020-01098-z

He, Q., Li, L. Z., Jing, X. W., Jiang, Y. G., & Yan, D. J. (2023). Impact resistance analysis and multi-objective optimization of polyurea-coated auxetic honeycomb sandwich panels. *Materials Today Communications, 35*, 105577. https://doi.org/10.1016/j.mtcomm.2023.105577

He, W. T., Lu, S. J., Yi, K., Wang, S. Q., Sun, G. Y., & Hu, Z. Q. (2019). Residual flexural properties of CFRP sandwich structures with aluminum honeycomb cores after low-velocity impact. *International Journal of Mechanical Sciences, 161–162*, 105026. https://doi.org/10.1016/j.ijmecsci.2019.105026

Hou, Y., Tai, Y. H., Lira, C., Scarpa, F., Yates, J. R., & Gu, B. (2013). The bending and failure of sandwich structures with auxetic gradient cellular cores. *Composites Part A: Applied Science and Manufacturing, 49*, 119-131. https://doi.org/10.1016/j.compositesa.2013.02.007

Li, W. T., Atsushi, D., Oh, Y. H., Jirathearanat, S., Wu, Z. A., & Chua, B. W. (2022). Influences of skin thickness, core topology, depth and direction on flexural deformation and ductile failure of Al honeycomb-based sandwich structures. *Composites Part B-Engineering, 239*, 109957. https://doi.org/10.1016/j.compositesb.2022.109957

Li, Z. J., Wen, Y. F., Wen, X. L., Hao, H., & Chen, W. S. (2023). Single and double-layered kirigami corrugated sandwich panels against impact loads. *Structures, 51*, 402-414. https://doi.org/10.1016/j.istruc.2023.03.074

Luo, H. C., Ren, X., Zhang, Y., Zhang, X. Y., Zhang, X. G., Luo, C., Cheng, X., & Xie, Y. M. (2022). Mechanical properties of foam-filled hexagonal and re-entrant honeycombs under uniaxial compression. *Composite Structures, 280*, 114922. https://doi.org/10.1016/j.compstruct.2021.114922

Lv, W. T., Li, D., & Dong, L. (2020). Study on mechanical properties of a hierarchical octet-truss structure. *Composite Structures, 249*, 112640. https://doi.org/10.1016/j.compstruct.2020.112640

Ma, M. Z., Yao, W. X., Jiang, W., Jin, W., Chen, Y., & Li, P. (2021). A multi-area fatigue damage model of composite honeycomb sandwich panels under three-point bending load. *Composite Structures, 261*, 113603. https://doi.org/10.1016/j.compstruct.2021.113603

Naresh, K., Cantwell, W. J., Khan, K. A., & Umer, R. (2021). Single and multi-layer core designs for pseudo-ductile failure in honeycomb sandwich structures. *Composite Structures, 256*, 113059. https://doi.org/10.1016/j.compstruct.2020.113059

Ni, X.H., Jiang, W., Zhang, X.G., Han, D., Teng, X.C., Hao, J., Xu, H.H., & Ren, X. (2023). Quasi-static and dynamic properties studies of a metamaterial with enhanced auxeticity and tunable stiffness. *Composite Structures, 321*, 117254. https://doi.org/10.1016/j.compstruct.2023.117254

Pan, J. W., Zhang, Q., Li, M., & Cai, J. G. (2024). A novel misplaced reinforced honeycomb with in-plane bidirectional enhancement. *International Journal of Mechanical Sciences, 270*, 109088. https://doi.org/10.1016/j.ijmecsci.2024.109088

Peliński, K., & Smardzewski, J. (2022). Static response of synclastic sandwich panel with auxetic wood-based honeycomb cores subject to compression. *Thin-Walled Structures, 179*, 109559. https://doi.org/10.1016/j.tws.2022.109559

Ren, X., Shen, J. H., Tran, P., Ngo, T. D., & Xie, Y. M. (2018). Design and characterisation of a tuneable 3D buckling-induced auxetic metamaterial. *Materials and Design, 139*, 336-342. https://doi.org/10.1016/j.matdes.2017.11.025

Rubino, V., Deshpande, V. S., & Fleck, N. A. (2010). The three-point bending of Y-frame and corrugated core sandwich beams. *International Journal of Mechanical Sciences, 52*, 485-494. https://doi.org/10.1016/j.ijmecsci.2009.11.009

Sun, Z., Chen, H. J., Song, Z. W., Liu, H. Y., Cui, R. H., Guo, X., & Shi, S. S. (2021). Three-point bending properties of carbon fiber/honeycomb sandwich panels with short-fiber tissue and carbon-fiber belt interfacial toughening at different loading rate. *Composites Part A: Applied Science and Manufacturing, 143*, 106289. https://doi.org/10.1016/j.compositesa.2021.106289

Vidwans, A., Trovalusci, P., Fantuzzi, N., & José, A. F. O. C. (2023). Application of column buckling theory to steel aluminium foam sandwich panels. *Structures, 54*, 607-617. https://doi.org/10.1016/j.istruc.2023.04.112

Wang, L., Sun, J., Ding, T., Liang, Y., Ho, J. C. M., & Lai, M. H. (2022). Manufacture and behaviour of innovative 3D printed auxetic composite panels subjected to low-velocity impact load. *Structures, 38*, 910-933. https://doi.org/10.1016/j.istruc.2022.02.033

International Journal of Engineering Research and Science & Technology

ISSN 2319-5991 www.ijerst.com

Vol. 20, Issue 1, 2024

Wang, Z. G., Li, Z. D., & Xiong, W. (2019a). Experimental investigation on bending behavior of honeycomb sandwich panel with ceramic tile face-sheet. *Composites Part B-Engineering, 164*, 280-286. https://doi.org/10.1016/j.compositesb.2018.10.077

Wang, Z. G., Li, Z. D., & Xiong, W. (2019b). Numerical study on three-point bending behavior of honeycomb sandwich with ceramic tile. *Composites Part B-Engineering, 167*, 63-70. https://doi.org/10.1016/j.compositesb.2018.11.108

Xia, F. K., Durandet, Y., Tan, P. J., & Ruan, D. (2022b). Three-point bending performance of sandwich panels with various types of cores. *Thin-Walled Structures, 179*, 109723. https://doi.org/10.1016/j.tws.2022.109723

Xia, F. K., Pang, T., Sun, G. Y., & Ruan, D. (2022a). Longitudinal bending of corrugated sandwich panels with cores of various shapes. *Thin-Walled Structures, 173*, 109001. https://doi.org/10.1016/j.tws.2022.109001

Xu, H. H., Luo, H. C., Zhang, X. G., Jiang, W., Teng, X. C., Chen, W. Q., Yang, J., Xie, Y. M., & Ren, X. (2023). Mechanical properties of aluminum foam filled re-entrant honeycomb with uniform and gradient designs. *International Journal of Mechanical Sciences, 244*, 108075. https://doi.org/10.1016/j.ijmecsci.2022.108075

Yan, Z. C., Liu, Y., Yan, J. B., Wang, B. C., Bai, F., Shi, Z. Q., & Huang, F. L. (2022). Anti-blast performance of 3D-printed sandwich panels with auxetic hexagonal and regular hexagonal honeycomb cores. *Engineering Structures, 272*, 114996. https://doi.org/10.1016/j.engstruct.2022.114996

Zhang, C. B., Lu, F. C., Wu, J., Zhang, K., Lin, B. C., & Qin, F. P. (2023). Research on three-point bending performance of hollow-core rod pyramidal gradient lattice sandwich beam. *Structures, 57*, 105165. https://doi.org/10.1016/j.istruc.2023.105165

Zhao, X., Wei, L. L., Wen, D. W., Zhu, G. H., Yu, Q., & Ma, Z. D. (2021). Bending response and energy absorption of sandwich beams with novel auxetic honeycomb core. *Engineering Structures, 247*, 113204. https://doi.org/10.1016/j.engstruct.2021.113204